The importance of unsaturated soil properties in the development of slope susceptibility map for Old Alluvium in Singapore

Harianto Rahardjo[1*], *Yangyang* Li[2], and *Alfrendo* Satyanaga[3]

[1]School of Civil and Environmental Engineering, Nanyang Technological University, 50 Nanyang Avenue, Singapore
[2]Monash Suzhou Research Institute, Monash University, Suzhou Industrial Park, Suzhou, China, formerly School of Civil and Environmental Engineering, Nanyang Technological University, 50 Nanyang Avenue, Singapore
[3]Department of Civil and Environmental Engineering, Nazarbayev University University, 53 Kabanbay Batyr, Kazakhstan

Abstract. Slope failures caused by rainfall are a regular occurrence in residual soils. As a result of climate change, increased precipitation is anticipated; preventing slope failures due to rain is therefore essential. One typical technique for pinpointing regions at risk for slope failures is the use of a "slope susceptibility map." Because the groundwater table is usually deep, many slopes in residual soil are typically unsaturated. Soil-water characteristic curve, permeability function, and unsaturated shear strength are the essential unsaturated soil parameters that should be factored into the creation of a slope susceptibility map. This research involved the Old Alluvium region in Singapore as a case study. Transient rainfall infiltration and grid-based regional slope stability (TRIGRS) model was used to establish pore-water pressure distributions over this region. Scoops3D was utilized to include the pore-water pressures calculated by TRIGRS for evaluating slope stability in three dimensions. To assess the reliability of the developed slope susceptibility map, two-dimensional (2-D) numerical analyses were performed on a subset of historically unstable residual soil slopes at the Bidadari site. Minimum safety factors determined via numerical analyses of the slopes under study agreed well with those determined via the slope susceptibility map.

1 Introduction

Altered rainfall patterns have been found in many areas of the world because of global warming [1]. As the average temperature increases, more evaporation and transpiration occur and hence the rainfall becomes more intense. Singapore is one of those areas where higher precipitation has been observed and anticipated [2].

Under a hot and humid climate, rocks in Singapore have been extensively weathered [3]. As a result of in-situ weathering of rocks, residual soils in Singapore commonly exist in unsaturated conditions due to the deep groundwater table (GWT) [4,5]. Soils in unsaturated conditions have additional shear strength contributed by the matric suction [6]. However, this additional shear strength contributed by the matric suction would decrease with an increase in moisture content when rainwater infiltrates into the soil [6]. Therefore, rainwater infiltration has been identified as the main factor that triggers slope failures in Singapore.

Slope failure can cause social and economic damages hence it is crucial to recognise the slopes that are prone to failures and apply measures to prevent slope failures. Most of the research on seepage and slope stability analyses using numerical modelling mainly focus on studying individual slopes. Some commonly used commercial software are PLAXIS LE, PLAXIS 2D, Geo-studio (SEEP/W, SLOPE/W), Slide2D and RS2 [7–10]. However, these programmes may fail to be utilised for a large-scale assessment of a region. In comparison, regional analysis involves analysis of a particular zone, which encompasses different terrain factors and groundwater conditions. Regional analyses can be effective in identifying specific locations of concern where slopes are more prone to failures within a region.

To identify the locations that are susceptible to slope failures within a region before performing further investigation and applying preventive measures, the development of a slope susceptibility map would be important. Past research studies have employed either qualitative or quantitative approaches to generate slope susceptibility maps [11–13]. Qualitative approaches like the analytical hierarchy process (AHP) method are more subjective which require the rank and weight of the influencing factors that largely rely on the judgement of the researchers [13]. On the other hand, quantitative approaches like statistical, machine learning and deterministic methods are based on objective equations which in general have better results in comparison to qualitative methods [14–16]. Deterministic methods such as the physically based models were considered as

* Corresponding author: chrahardjo@ntu.edu.sg

the advanced methods as they simulate the physical processes based on the physical laws. Researchers found that deterministic methods performed slightly better than the other models [17–20]. The main advantage of the physically based models over the statistical models and machine learning models is that information on historical slope failures is not required in the physically based models. When using the statistical models and machine learning models, reliable results may not be obtained when large datasets on historical slope failures are not available.

The physically based models that have been adopted to predict the regional rainfall-induced slope instability in past research are mostly infinite slope stability models, such as the Transient rainfall infiltration and grid-based regional slope stability (TRIGRS) [21,22], Shallow landslide and stability model (SHALSTAB) [23] and Stability index mapping (SINMAP) [24]. However, these models assume that the failure mode is translational, and the slip surface is parallel to the slope surface with a shallow depth. To overcome this limitation, Scoops3D model was proposed to carry out three-dimensional (3-D) slope stability analyses [25]. Scoops3D performs 3-D slope stability analyses by adopting the 3-D method of column limit equilibrium analysis. Before carrying out slope stability analyses using Scoops3D, TRIGRS have been adopted to compute transient pore pressure change due to rainfall infiltration [26–28].

When studying rainfall-induced slope failures, unsaturated soil mechanics are very important and should be incorporated into the analyses for residual soil slopes with deep GWT [28,29]. The hydraulic conductivity and shear strength of unsaturated soils are highly dependent on the soil water content. Therefore, this study aims to propose a slope susceptibility map for Old Alluvium in Singapore by incorporating unsaturated soil mechanics principles. Old Alluvium (semi-hardened alluvial deposits) in the east, together with Bukit Timah Granite (igneous rocks) in the north and central-north, and Jurong Formation (sedimentary rocks) in the west, are the three major geological formations in Singapore [30].

This research employed Old Alluvium region in Singapore as a case study, using TRIGRS model to establish pore-water pressure distributions over this region. Scoops3D was utilized to include the pore-water pressures calculated by TRIGRS for evaluating slope stability in three dimensions. TRIGRS and Scoops3D were selected as they are deterministic models that can compute the transient pore-water pressure changes and 3-D slope stability with the incorporation of unsaturated soil properties. Two-dimensional (2-D) numerical analyses were performed on a subset of historically unstable residual soil slopes at Bidadari site to validate the factor of safety (FoS) from the slope susceptibility map. The 2-D analyses were performed using SEEP/W and SLOPE/W with the unsaturated soil properties from laboratory tests on the soil from Bidadari Park Drive.

2 Slope susceptibility mapping for Old Alluvium

TRIGRS programme [22] was used in this study to compute the transient pore-water changes due to rainwater infiltration. Analytical solutions of the Richards equation for the one-dimensional (1-D) vertical flow through unsaturated soils are adopted by TRIGRS to estimate ground surface infiltration. As for the soil-water characteristic curve (SWCC) and permeability function, Gardner's models [31] are applied in TRIGRS. With the spatial distributions of pressure heads obtained from the TRIGRS analyses, Scoops3D [25] was used to evaluate the regional slope stability. The stability is assessed based on rotational and spherical slip surfaces.

A slope at the Bidadari site (Fig.1) in the Old Alluvium Formation was used to validate the slope stability results. Therefore, Zone A which consists of the Bidadari site was selected for the regional analyses. 1-D seepage analyses were carried out first using TRIGRS to obtain the pore-water pressure distributions. Extreme historical rainfall was applied, which is 353 mm/day in Singapore based on the historical data from 1972 to 2017 [32]. The digital elevation model (DEM), slope angle, flow direction and GWT maps of Zone A were used as the input layers for TRIGRS analyses. The average soil properties for Zone A were used in the analyses [32] (Table 1).

Table 1. Properties of soil for TRIGRS at Zone A within Old Alluvium.

TRIGRS Parameters	Zone A
c' (kPa)	8.3
ϕ' (°)	34
Bulk unit weight (kN/m^3)	19.6
Saturated permeability, k_s (m/s)	1.0e-04
Coefficient of diffusivity (m^2/s)	8.3e-04
Gardner's α	0.29543

Pore-water pressure results from TRIGRS were then exported to Scoops3D to calculate slope stability. By classifying the FoS results from Scoops3D into four risk categories (i.e., low, moderate, high, and very high risks), the slope susceptibility map for Zone A (Fig.2) was then obtained. Slopes with a FoS above 1.5 are at low risk of slope failures while slopes with a FoS below 1 are at very high risk of slope failures. In between, there are slopes at high risk with a FoS from 1 to 1.25 and moderate risk with FoS from 1.25 to 1.5. As shown in the slope susceptibility map, most areas are classified with low risks of slope failures (in green colour). The location of the Bidadari site was also marked out. Based on the map, the Bidadari slope has a FoS of 1.64, which is classified as a low-risk slope.

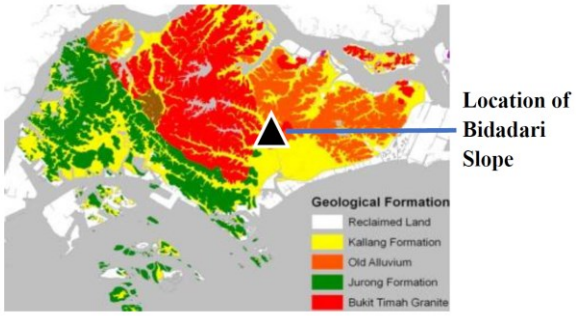

Fig. 1. Location of the investigated slope for validation of map.

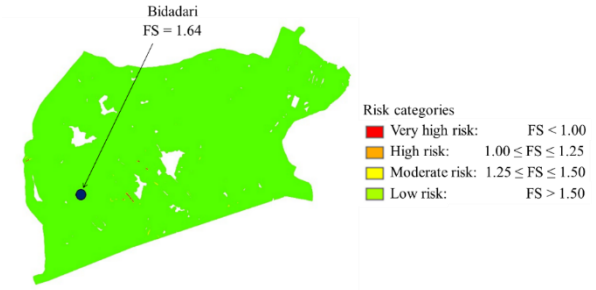

Fig. 2. Slope susceptibility map for Zone A at Old Alluvium.

3 Validation of map

A slope at the Bidadari site was selected for the validation of the results from the regional analyses. Soil samples from the Bidadari slope were obtained from boreholes. Table 2 lists the index properties of the samples from depths of 3-4m and 5-6m. Based on the borelog report from this slope, soil properties from depths 3-4 m can be used to represent layer 1 while soil properties from depths 5-6 m can be used to represent the second layer of the soil slope.

Table 2. Index properties of soil at Bidadari slope.

Index Properties	Bidadari (3-4m)	Bidadari (5-6m)
USCS	SC	SC
Gravel (%)	2	1
Sand (%)	69	55
Fines (%)	29	44
Bulk density (Mg/m^3)	1.90	1.91
Specific Gravity, G_s	2.68	2.53
Water content, *w* (%)	31	29
Liquid Limit, LL (%)	67	64
Plastic Limit, PL (%)	26	29
Plastic Index, PI (%)	41	35
Saturated permeability, k_s (m/s)	7.0e-6	2.0e-6

Following ASTM D6836-16 [33], a small-scale centrifuge, pressure plate and chilled-mirror hygrometer were used to obtain the SWCC data points at suctions below 250 kPa, medium suctions from 250 kPa to 500 kPa and high suctions up to 100 MPa, respectively. The SWCC data were then best fitted using 1) Satyanaga et al.'s equation [34] for bimodal SWCC in the case of the 3-4 m sample (Fig.3), and 2) Fredlund and Xing's equation [35] for unimodal SWCC in the case of the 5-6 m sample (Fig.4). Then, the permeability functions were obtained using a statistical method and Leong and Rahardjo's best-fitting equation [36] for permeability (Fig.5).

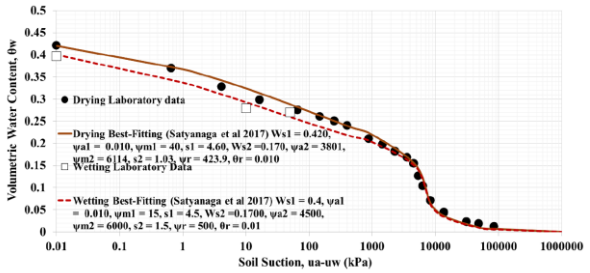

Fig. 3. SWCC for layer 1 at Bidadari slope.

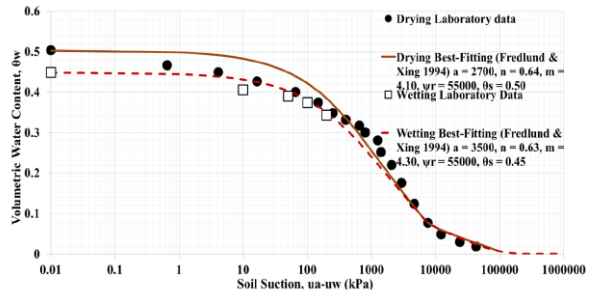

Fig. 4. SWCC for layer 2 at Bidadari slope.

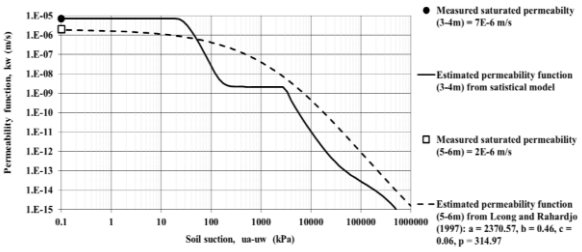

Fig. 5. Unsaturated permeability for soil at Bidadari slope.

The shear strength parameters are summarised in Table 3. The saturated shear strength parameters (effective cohesion c′ and effective friction angle ϕ') were obtained by performing consolidated undrained (CU) Triaxial tests with pore-water pressure measurements following ASTM 4767-11 [37] and the unsaturated shear strength parameters ϕ^b was obtained from multistage consolidated drained (CD) triaxial tests [38].

Table 3. Shear strength properties of soil at Bidadari slope.

Index Properties	Bidadari first layer (0-5m)	Bidadari second layer (>5m)
c′ (kPa)	11	11
ϕ′ (°)	34	34
ϕ^b (°)	25	17

With the soil properties obtained from the laboratory tests, 2-D seepage analyses using GeoStudio SEEP/W were carried out first using the SWCCs and permeability functions of the soils. The geometry and the applied boundary conditions are shown in Fig.6. The GWT depths were estimated from the measurements of piezometers. The extreme historical daily rainfall (i.e., 353 mm/day) was applied for one day and followed by the subsequent day with no rain to simulate a one-day rainfall event and the following recovery period, respectively. Constant total heads of 26.7 m and 20.5 m were imposed at the left and right sides below the GWT, respectively. At the two sides above the GWT, no flow condition was applied.

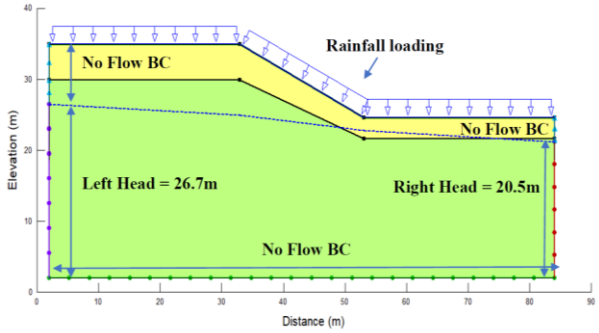

Fig. 6. Boundary conditions for Bidadari slope for seepage analyses using SEEP/W.

Pore-water pressure results from SEEP/W were then imported to SLOPE/W for the 2-D slope stability analyses. As illustrated in Fig.7, to efficiently minimise the boundary effect in slope stability analyses, the studied region was extended both horizontally and vertically by at least three times the slope height from the crest and toe of the slope [39].

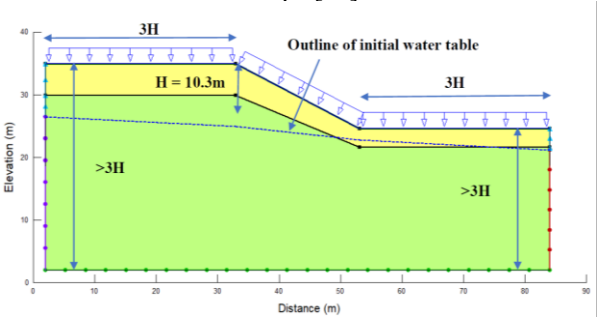

Fig. 7. 2-D numerical model for slope stability at Bidadari.

The variations in FoS based on the application of the historical maximum daily rainfall are presented in Fig.8. The FoS based on the historical maximum rainfall decreases significantly to the minimum value of 1.76. The slope recovers gradually to FoS of 1.82 at 24 hours after the end of rainfall.

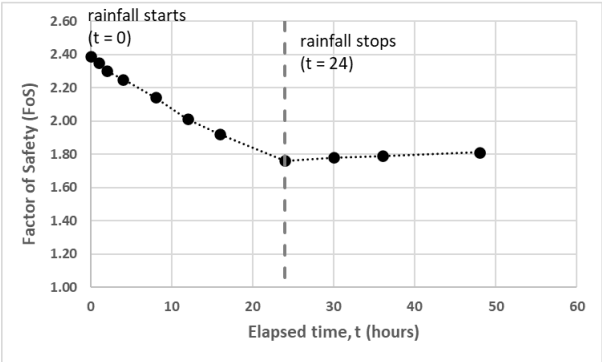

Fig. 8. Factor of safety variations of slope at Bidadari under maximum daily rainfall.

In comparison to the computed FoS of 1.64 at Bidadari slope from the regional analyses using TRIGRS and Scoops3D, the FoS obtained from the 2-D analyses using SEEP/W and SLOPE/W is slightly higher with a value of 1.76. Though the FoS obtained from both analyses resulted in the same low-risk class, the main reason for the difference in FoS (i.e., 7.32%) could be attributed to the variability in the saturated permeability within the zone. The average saturated permeability for Zone A as used in the regional analyses is 1e-04 m/s while the laboratory results show that the saturated permeability at the Bidadari slope is much lower (i.e., from 2e-06 to 7e-06 m/s). The variability in the saturated permeability within the zone could be high, causing the average permeability of the zone to be higher than that at Bidadari site. Previous research by Rahardjo et al. [40] showed that residual soil slopes of higher saturated coefficient of permeability would have a lower minimum FoS as the k_s parameter is considered to play a dominant role in rainfall infiltration. This could explain why a lower FoS was observed from the regional analyses with a higher saturated permeability, as compared to the FoS from the 2-D analyses with a lower saturated permeability. However, this high variability in permeability only resulted in a 7.32% difference in the final computed FoS from Scoops3D and SLOPE/W (i.e., 1.64 and 1.76, respectively). This is due to the fact that the shear strength parameters and the slope geometry (i.e., slope height and slope angle) also play important roles in controlling the stability of residual soil slope.

4 Conclusions

As a case study in Singapore, this research developed a slope susceptibility map under the historical maximum daily rainfall for a zone in Old Alluvium. With the pore-water pressure distributions exported from the regional 1-D seepage analyses using TRIGRS, Scoops3D was used to compute the 3-D regional slope stability for the zone as part of the slope susceptibility map. The regional analyses incorporated unsaturated soil mechanics and

the average soil properties of the zone were used. The factor of safety of the Bidadari slope within the zone was 1.64 and classified as at low risk from the slope susceptibility map. 2-D seepage and slope stability analyses on this Bidadari slope were subsequently carried out to validate the slope susceptibility map generated from the regional analyses. The saturated and unsaturated soil properties from the laboratory tests were used in the 2-D analyses. The minimum factor of safety determined from 2-D analyses of the slope was 1.76, which agreed well with, though slightly higher than that determined from the slope susceptibility map. The lower FoS obtained from the regional analyses may be due to the higher mean saturated permeability of the overall soil within the zone than that of the Bidadari slope. The average saturated permeability used in TRIGRS is likely not representative of that at the Bidadari slope. However, this difference in soil properties did not affect much in the slope stability results for the Bidadari slope as obtained from the regional analyses and 2-D analyses. This similarity could be attributed to the similar slope geometry studied and shear strength properties used in the analyses. Slope geometry and shear strength properties also play an important role in controlling the stability of residual soil slopes. This case study demonstrates an applicable and reliable way to generate slope susceptibility maps from regional analyses using TRIGRS for 1-D seepage analyses and Scoops3D for 3-D slope stability analyses. The generated slope susceptibility maps help in quickly pinpointing locations that are more prone to rainfall-induced slope failures before further investigations and prevention works are carried out.

References

1. J. Lehmann, D. Coumou, and K. Frieler, Clim. Change **132**, 501 (2015)
2. X. Li, X. Wang, and V. Babovic, Int. J. Climatol. **38**, 125 (2018)
3. Y. Li, A. Satyanaga, S. Rangarajan, H. Rahardjo, and D. T.-T. Lee, in *Soils Urban Ecosyst.*, edited by A. Rakshit, S. Ghosh, V. Vasenev, H. Pathak, and V. D. Rajput (Springer Singapore, Singapore, 2022), pp. 321–335
4. J. Pitts, Q. J. Eng. Geol. **17**, 93 (1984)
5. H. Rahardjo, A. S. Nio, E. C. Leong, and N. Y. Song, J. Geotech. Geoenvironmental Eng. **136**, 1555 (2010)
6. D. G. Fredlund, N. R. Morgenstern, and R. A. Widger, Can. Geotech. J. **15**, 313 (1978)
7. J. W. Mburu, A.-J. Li, H.-D. Lin, and C.-W. Lu, Sustainability **14**, 14465 (2022)
8. P. Das, D. Patwa, V. G., and T. V. Bharat, Bull. Eng. Geol. Environ. **81**, 194 (2022)
9. H. Rahardjo, Y. Kim, and A. Satyanaga, Int. J. Geo-Eng. **10**, 8 (2019)
10. Y. Li, A. Satyanaga, and H. Rahardjo, Int. Soil Water Conserv. Res. **9**, 405 (2021)
11. A. Shirzadi, K. Soliamani, M. Habibnejhad, A. Kavian, K. Chapi, H. Shahabi, W. Chen, K. Khosravi, B. Thai Pham, B. Pradhan, A. Ahmad, B. Bin Ahmad, and D. Tien Bui, Sensors **18**, 3777 (2018)
12. G. Formetta, G. Capparelli, and P. Versace, Hydrol. Earth Syst. Sci. **20**, 4585 (2016)
13. A. El Jazouli, A. Barakat, and R. Khellouk, Geoenvironmental Disasters **6**, 3 (2019)
14. P. Reichenbach, M. Rossi, B. D. Malamud, M. Mihir, and F. Guzzetti, Earth-Sci. Rev. **180**, 60 (2018)
15. L.-J. Wang, M. Guo, K. Sawada, J. Lin, and J. Zhang, Geosci. J. **20**, 117 (2016)
16. B. Pradhan, M. I. Seeni, and B. Kalantar, in *Laser Scanning Appl. Landslide Assess.*, edited by B. Pradhan (Springer International Publishing, Cham, 2017), pp. 193–232
17. L. Cascini, Eng. Geol. **102**, 164 (2008)
18. L. Cascini, M. Ciurleo, S. Di Nocera, and G. Gullà, Geomorphology **241**, 371 (2015)
19. G. Sorbino, C. Sica, and L. Cascini, Nat. Hazards **53**, 313 (2010)
20. M. Ciurleo, L. Cascini, and M. Calvello, Eng. Geol. **223**, 71 (2017)
21. R. M. Iverson, Water Resour. Res. **36**, 1897 (2000)
22. R. L. Baum, W. Z. Savage, and J. W. Godt, *TRIGRS - A Fortran Program for Transient Rainfall Infiltration and Grid-Based Regional Slope-Stability Analysis, Version 2.0* (2008)
23. D. R. Montgomery and W. E. Dietrich, Water Resour. Res. **30**, 1153 (1994)
24. R. T. Pack, D. G. Tarboton, and C. N. Goodwin, in (1998)
25. M. E. Reid, S. B. Christian, D. L. Brien, and S. Henderson, Tech. Methods (2015)
26. J. He, H. Qiu, F. Qu, S. Hu, D. Yang, Y. Shen, Y. Zhang, H. Sun, and M. Cao, CATENA **197**, 104999 (2021)
27. T. V. Tran, M. Alvioli, G. Lee, and H. U. An, Landslides **15**, 1071 (2018)
28. A. Satyanaga and H. Rahardjo, Proc. Inst. Civ. Eng. - Geotech. Eng. **175**, 276 (2022)
29. C. W. W. Ng and Q. Shi, Q. J. Eng. Geol. **31**, 105 (1998)
30. S. P. W. Department and S. P. W. D. G. Unit, *Geology of the Republic of Singapore* (Public Works Department, 1976)
31. W. R. Gardner, Soil Sci. **85**, 228 (1958)
32. H. Rahardjo, E. C. Leong, X. S. Qin, A. Satyanaga, M. Nistor, Y. Kim, and Z. H. Koh, *The Development of Slope Management and Susceptibility Geographical Information System* (2020), p. 60
33. ASTM International, *Test Methods for Determination of the Soil Water Characteristic Curve for Desorption Using Hanging Column, Pressure Extractor, Chilled Mirror Hygrometer, or Centrifuge* (2018)
34. A. Satyanaga, H. Rahardjo, E.-C. Leong, and J.-Y. Wang, Comput. Geotech. **48**, 51 (2013)
35. D. G. Fredlund and A. Xing, Can. Geotech. J. **31**, 521 (1994)

36. E. C. Leong and H. Rahardjo, J. Geotech. Geoenvironmental Eng. **123**, 1118 (1997)
37. ASTM International, *Test Method for Consolidated Undrained Triaxial Compression Test for Cohesive Soils* (2011)
38. D. G. Fredlund and H. Rahardjo, *Soil Mechanics for Unsaturated Soils: Fredlund/Soil Mechanics for Unsaturated Soils* (John Wiley & Sons, Inc., Hoboken, NJ, USA, 1993)
39. I. Tsaparas, H. Rahardjo, D. G. Toll, and E. C. Leong, Comput. Geotech. **29**, 1 (2002)
40. H. Rahardjo, T. H. Ong, R. B. Rezaur, and E. C. Leong, J. Geotech. Geoenvironmental Eng. **133**, 1532 (2007)